A High Power Electrodeless Plasma Thruster Operated with a FET-Based Inverter Power Supply

IEPC-2015-87／ISTS-2015-b-87

Presented at Joint Conference of 30th International Symposium on Space Technology and Science
34th International Electric Propulsion Conference and 6th Nano-satellite Symposium,
Hyogo-Kobe, Japan
July 4 – 10, 2015

Takayoshi Ishiyama[1], Aiki Chiba[2], Kazunori Takahashi[3], Atsushi Komuro[4], and Akira Ando[5]
Department of Electrical Engineering, Tohoku University, Sendai-Miyagi, 980-8579, Japan

Abstract: An electrodeless plasma thruster is newly constructed and operated with high radio frequency (RF) power. A field effect transistor (FET) based inverter power supply is provided as an RF source instead of widely used conventional 13.56 MHz RF power supplies. The inverter source drives RF power up to 21 kW with the frequency of several hundreds kHz. It converts direct current (DC) to RF with the efficiency of about 90 %. Thrust is directly measured using a plate type thrust target. In the preliminary experiments, the maximum thrust of 20 mN is obtained with RF power of 16 kW using argon gas as a propellant. At that time, the obtained plasma densities are 7×10^{18} m^{-3} in the source tube and 4×10^{17} m^{-3} at the target position.

Nomenclature

A	=	plasma cross-section area
B	=	external applied magnetic field strength
F_t	=	force measured by the load cell
I_t	=	impulse bit
I_{cal}	=	supplied current to the calibration coil
Kti	=	calibration coefficient for impulse bit
P_{RF}	=	system input power
V_c	=	charge voltage
V_{RF}	=	RF voltage
Z	=	distance from the source exit
m_{dot}	=	mass flow rate
r	=	radial distance from the centerline
r_p	=	plasma radius
ΔV	=	LED sensor output
α	=	calibration coefficient for steady state magnetic force
δt	=	time width of the pulse current supplied to the calibration coil
δV	=	LED sensor output of the first swing of the target

[1] Graduate Student, Department of Electrical Engineering, itakayoshi@ecei.tohoku.ac.jp.
[2] Graduate Student, Department of Electrical Engineering, chiba@ecei.tohoku.ac.jp.
[3] Associate Professor, Department of Electrical Engineering, kazunori@ecei.tohoku.ac.jp.
[4] Assistant Professor, Department of Electrical Engineering, komuro@ecei.tohoku.ac.jp.
[5] Professor, Department of Electrical Engineering, akira@ecei.tohoku.ac.jp.

I. Introduction

As space technologies have been drastically developed, more research and experiments related to deep space missions and/or manned interstellar missions have been conducted. These missions demand long-lived propulsion system with large thrust and high specific impulse. So far, various types of electrical propulsion devices have been proposed, and some of them have been widely employed from attitude control to keep operation orbits for artificial satellites to maneuver for space missions.

However, since electrodes in conventional propulsion devices such as a magnetoplasma dynamic thruster[1] and a Hall effect thruster[2] are exposed to source plasmas, the electrode erosion is the inevitable issue, which has to be addressed to achieve the above-mentioned missions. Lifetime of the μ10 ion engine for the Hayabusa has been successfully improved by utilizing an electrodeless microwave discharge for the plasma production[3]. The Variable Specific Impulse Magneto-plasma Rocket (VASIMR) engine has also been invented as a fully electrode-less thruster[4]. The VASIMR consists of three sections: plasma production section via a helicon wave discharge, ion cyclotron resonant heating (ICRH) section, and magnetic nozzle section, where the electric power is directly coupled with plasma ions. Since the strong magnetic field (~ 1 T) for the resonance can also guide the plasma along the high aspect ration source tube, it is expected that the plasma loss to the wall be simultaneously inhibited.

Another fully electrodeless thruster is a simple helicon plasma thruster; the electric power is efficiently coupled with only plasma electrons. The thruster is typically operated for the RF power less than a few kW and for the magnetic field less than ~ 0.1 T. Recent works have shown that the electron pressure is efficiently converted into the ion dynamic momentum through current-free double layer and/or ambipolar electric fields[5] and the accelerated ions are spontaneously neutralized by energetic electrons[6]. Furthermore, the recent individual measurements of the thrust components arising from the magnetic nozzle have suggested the additional thrust generation via a magnetic plasma expansion, which appears to be due to the interaction between the radial magnetic field and the electron diamagnetic drift current[7, 8]. More recent experiments have shown that a part of the axial plasma momentum is lost to the lateral wall[9]; it is expected that the presence of the long-distance lateral wall will lead loss of the momentum to the wall. More addressing the efficiency, the energy transfer efficiency to the plasma can be given by the product of the DC – RF conversion and RF plasma coupling efficiency. Therefore, it is useful to operate the helicon or inductively coupled plasma thruster with the efficient inverter type RF amplifier.

Here, the FET-based inverter type RF generator (maximum power of ~ 20 kW) is installed to the helicon type plasma thruster, which is tested by attaching the source contiguously to a diffusion chamber, instead of the 13.56 MHz RF generator generally used for helicon plasma production[10, 11]. The impedance matching is tunable by adjusting the driving frequency in the range of several hundreds of kHz. The thruster performance is assessed by a pendulum target technique and a Langmuir probe diagnosis. In section II, details of the experimental setup and

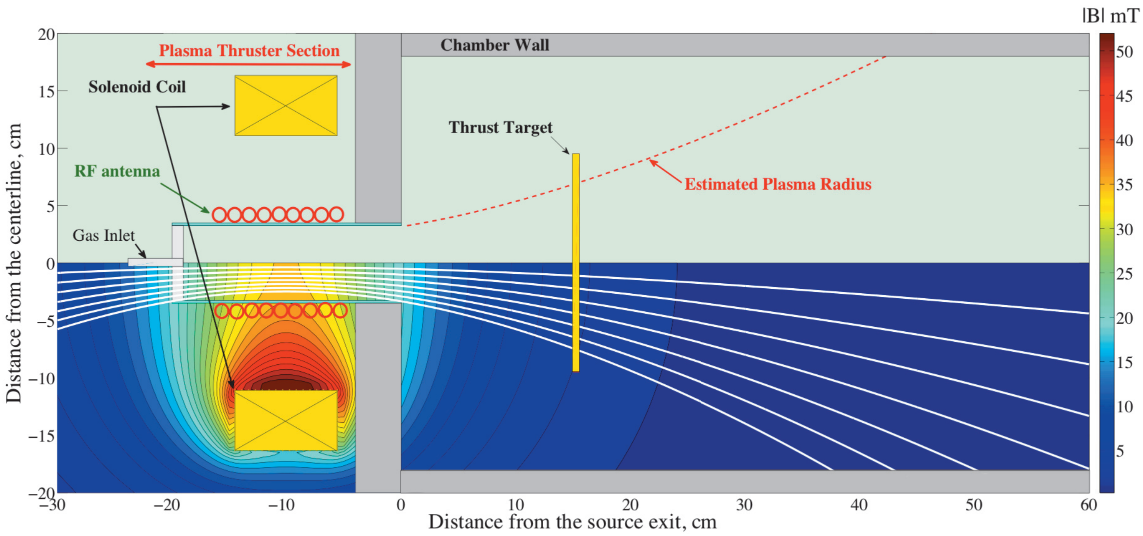

Figure.1 Plasma radius estimation (red dashed line) and the thrust target position (yellow rectangle) in the vacuum chamber (upper-side) and magnetic field strength (contour plot) and lines (solid lines) in the experimental apparatus for I_B = 10 A (lower-side)

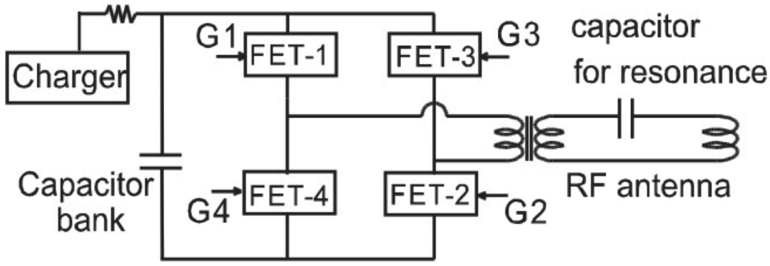

Figure. 2 An RF inverter power supply circuit with an impedance matching circuit and an RF antenna

diagnoses are shown. The results are described and discussed in section III. Conclusion and future works will be given in section IV.

II. Experiments

A. Experimental apparatus

All experiments are conducted using the vacuum device shown in Fig. 1. The test facility consists of a 40-cm-diameter and 60-cm-long cylindrical stainless steel vacuum chamber. The evacuation system consists of ULVAC ULK-06A oil diffusion pump with the pumping speed of 1100 l/s The base pressure of 5.0×10^{-7} Torr can be achieved. The chamber pressure is monitored by a crystal/cold cathode combination gauge CC-10 made by Tokyo electronics Co., Ltd and an ionization gauge made by ULVAC Japan. Ltd.

A plasma source is a cylindrical Pyrex® tube with 7 cm in diameter and 20 cm in length surrounded by a 9-turn loop antenna and is attached to the chamber. The antenna is connected to the inverter power supply MA – 15 KY that has a circuit shown in Fig. 2 made by Denki Kogyo Co., Ltd. This inverter includes a matching circuit and the matching frequency of the system is about 300 kHz. As shown in Fig.2, applied voltage to the RF antenna is adjusted by the voltage V_c of the charger in primary stage of the inverter and sent to the secondary stage via the step-down transformer. The transfer ratio is currently chosen as 4 to 1. Thus, applied RF voltage V_{RF} is estimated as $0.25V_c$. RF power is arbitrarily adjustable up to about 20 kW. Propellant gas is supplied from the gas inlet upstream of the source, and argon gas currently selected for the preliminarily test since the recent helicon thruster experiment shows no clear improvement by the propellant species[12]. The coordinate system is set to the axial direction and the radial direction. The origin of the axial direction Z = 0 cm is the source exit. Downstream of the source exit is defined as positive Z direction.

As shown in Fig. 1, a magnetic solenoid coil is set at Z = - 10 cm, where the dimensions are 11.5 cm width, 20 cm in inner diameter, and 33 cm in outer diameter, respectively. The coil is connected to a DC power supply and the solenoid current is increased up to 10 A. Figure 3 shows measured magnetic field strength at the center of the coil as a function of a solenoid current. As shown in Fig. 3, magnetic field strength at the center of the solenoid coil, (Z = - 10 cm and r = 0 cm) is proportional to the DC current and gives the field strength of 3.61 mT/A. In Fig. 1, magnetic field configuration is also shown in the experimental setup by contour plot and solid lines. From this figure, it can be observed that magnetic field lines are most compressed under the RF antenna, which is the plasma production area, and gradually expanding downstream. This field works as a magnetic nozzle to enhance thrust forces.

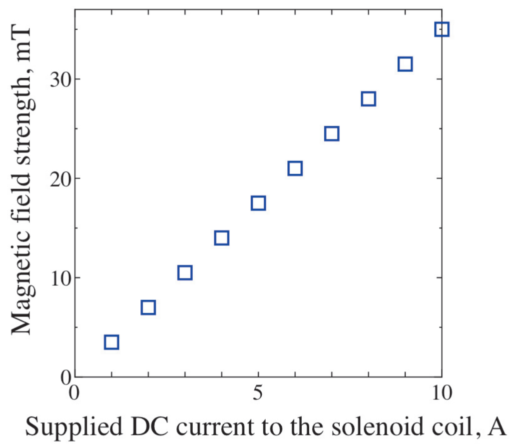

Figure 3. Magnetic field strength at the magnetic coil center

B. Target Calibration

In many cases of plasma thruster research including helicon thruster studies, a plasma source is put in a vacuum chamber and a thrust balance is used to directly measure thrust[13, 14]. Since the source tube is attached to the outside of the chamber in the present experiment, a thrust balance is not available. Therefore, a thrust target technique very similar to Ref. 13 is used for the thrust assessment. In Fig. 1, a target plate position and estimated plasma radius are shown with the experimental setup. Plasma expansion along the magnetic field lines is calculated from the following relation BA = constant, where B is magnetic field strength on the centerline and A is the plasma cross-section given by $A = \pi r_p^2$.

Figure 4 shows the schematic of the target structure. An insulator plate is attached to a pendulum, and its displacement is measured by a light emitted diode (LED) displacement sensor located just behind the insulator plate. The sensitivity and resolution of the LED sensor is 1.6 V/ mm ± 10 % and 5 μm, respectively. A permanent magnet and a metal block are attached to the left lower edge of the target frame unit and to the downstream side of the

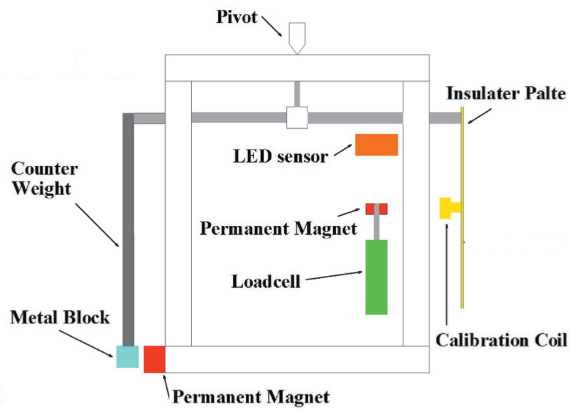

Figure. 4 Schematic of the thrust target structure

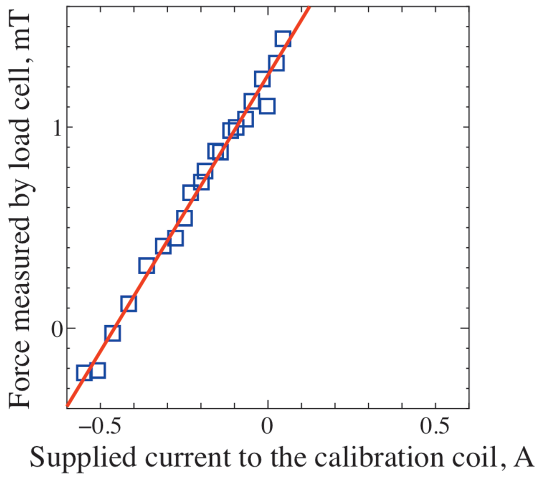

Figure. 5 The force F_t measured by the load cell (open squires) and their fitted line (red solid line) as a function of the calibration coil current I_{cal}.

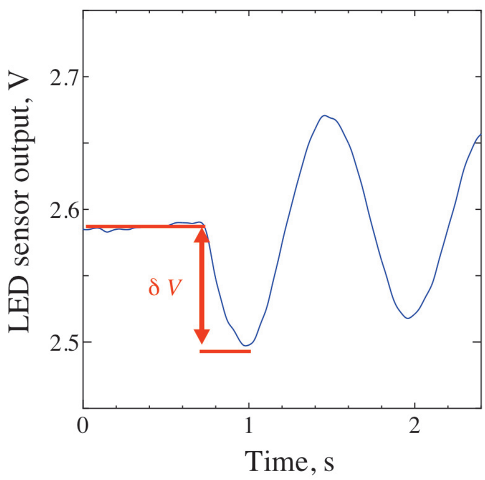

(a)

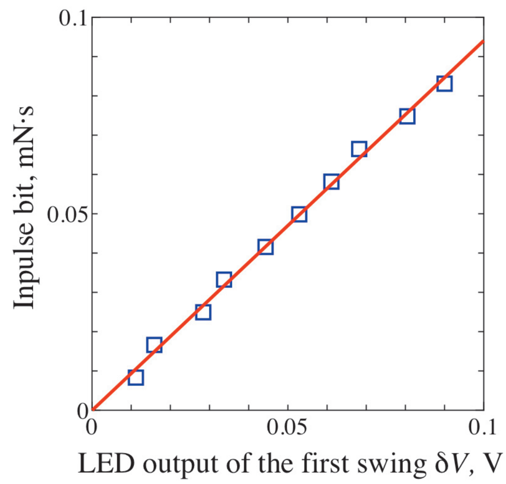

(b)

Figure. 6 (a) Typical signal of the LED sensor output for I_{sol} = 1 A and δt = 30 ms and (b) measured impulse bit (open squires) and their fitted line (red solid line) as a function of LED sensor output of the first swing of the thrust target

pendulum structure, respectively, in order to damp an oscillation of the target plate (called magnetic damper). The metallic block also works as a counter balance.

Target calibration coefficient is obtained from the same calibration method as Ref. 15. Very briefly, a calibration coil is attached to the backside of the target plate and a permanent magnet installed on a load cell is located just behind the target. When supplying a current to the coil, a magnetic field is generated there. The magnetic force acting on the permanent magnet is transferred to the load cell and the magnitude of the magnetic force is obtained from the load cell signal. At first, a DC calibration current I_{sol} is supplied to the calibration coil to obtain the calibration coefficient relating the DC current to the steady state force acting on the target, which is precisely controlled LabVIEW® program and amplified signal from the load cell is digitized by a high resolution data acquisition system. The current I_{sol} output from a function generator is amplified via a bipolar power unit in controlled current mode. At the same time, the amplified current is monitored by a current probe. The current is swept from -0.6 A to 0.1 A for 10 seconds. Figure 5 shows the calibration results relating the calibration current I_{cal} to the force F_t measured by the load cell. Open squire shows raw data and red solid line is a fitted line. The output signal shows a good linearity, although the force does not show zero force at zero current because the load cell may have been slightly inclined and detected the weight of the permanent magnet. Thus, the calibration coefficients is $\alpha \equiv F_t/I_{sol} \fallingdotseq 2.75$ mN/A, which is used to estimate the impulse bit imparted by the pulsed current of the calibration coil as explained in Ref. 15. After finishing the calibration for the steady state, calibration for the pulsed current is curried out. Impulse bit imparted on the target is calculated as $I_t = \alpha I_{sol}\delta t$. Figure 6 (a) shows the typical signal of the LED sensor output when pulsed current is sent to the coils. The amplitude of the first swing δV can be regarded as the displacement caused by the pulsed current from the initial state. The measurement is conducted for solenoid current up to 1 A with an increment of 0.1 A, and pulse width δt is 30 milliseconds. Figure 6 (b) shows the impulse bit as a function of the measured δV. From this figure, the calibration coefficient can be acquired as $K_{ti} \equiv I_t/\delta V \fallingdotseq 0.94$ mN·s /V. It should be mentioned that the LED sensor shows no displacement when both the DC and pulsed currents are supplied to the coil with no permanent magnet on the load cell.

III. Result and Discussion

Figure 7 shows the thrust force as a function of RF power P_{RF} for each mass flow rate when magnetic field strength of 27.4 mT is applied. RF power is calculated by multiplying RF voltage adjusted by charge voltage as aforementioned by the current flowing the RF antenna. The charge voltage is chosen as 100, 150, 200 and 250 V. From Fig. 7, it is clear that the thrust becomes larger as the input RF power becomes larger. Besides, the result shows different tendencies at the region less than 10 kW of RF power and higher region. At the lower region, where

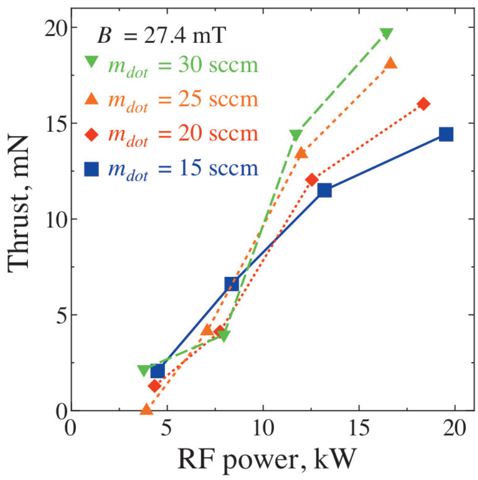

Figure. 7 Thrust as a function of RF power for each mass flow rate

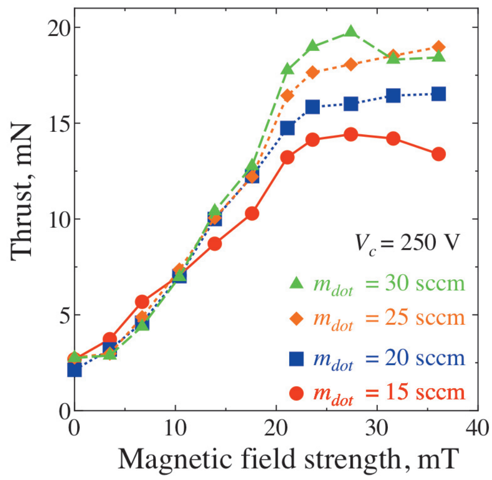

Figure. 8 Thrust as a function of magnetic field strength for each mass flow rate

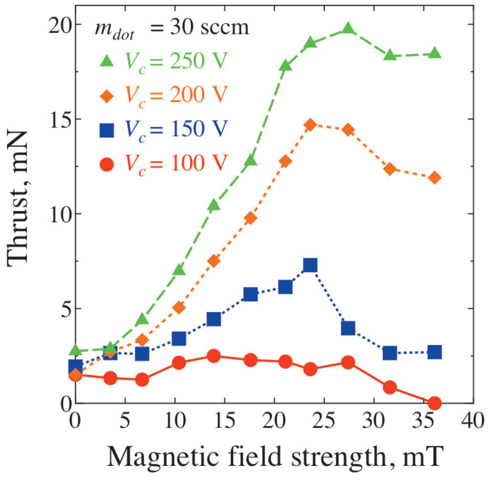

Figure. 9 Thrust as a function of magnetic field strength for each charging voltage

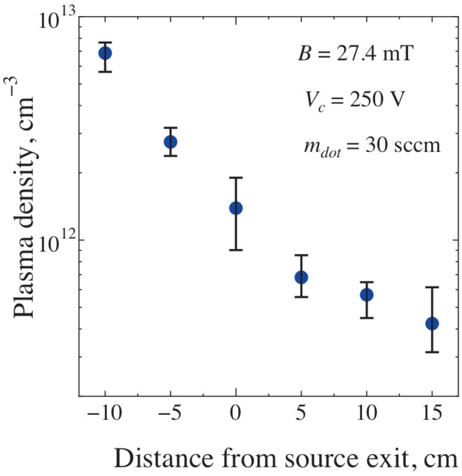

Figure. 10 Axial distribution of plasma density when magnetic field is 27.1 mT, mass flow rate is 30 sccm, and charge voltage is 250 V

100 and 150 V of charge voltages are applied, large changes of the thrust are observed regardless of the mass flow rate. When RF power increases more than 10 kW, where 200 and 250 V of charge voltage are applied, larger thrust is generated when more propellant gas are supplied. This indicates much plasma is produced by introducing more propellant to the source in higher RF power region.

Figures 8 and 9 show the thrust force as a function of magnetic field strength for each mass flow rate and each charge voltage, respectively. These figures also imply that larger thrust is acquired when the larger mass flow rate of the propellant is introduced and larger RF power is supplied as is in Fig. 7. It also shows that there is the optimized magnetic field strength where the thrust is saturated. In this case, the optimized magnetic field strength exists between 25 and 28 mT. The reason why the thrust is saturated or decreased at the stronger magnetic field region is that plasma coupling becomes worse by applying stronger field and plasma production is decreased. In this work, it is observed that it becomes difficult to ignite plasma when more than 30 mT of magnetic field is applied.

Figure 10 shows the axial distribution of plasma density between Z = -10 cm and 15 cm when the maximum thrust is given. The position of Z = -10 cm corresponds to just below the RF antenna, which is the plasma production area. Z = 0 cm is the source exit as defined, and Z = 15 cm is the target position, respectively. In the source, the density of 7×10^{18} m^{-3} is obtained at Z = -10 cm. It is also observed that the plasma density about 4×10^{17} m^{-3} is transported to the target. In this work, the maximum thrust is 19.7 mN when16.4 kW of the RF power is supplied with argon flow of 30 sccm, which corresponds to 8.92×10^{-7} kg/s and pressure in the chamber is 2.2 mTorr. At this moment, the thrust power ratio is 1.2 mN/kW, which is much lower than those in other works[16]. To enhance the performance of this thruster, it is necessary to suppress the plasma loss same as other types of electrodeless thrusters. It is thought that this problem can be solved by adjusting the magnetic field configuration and/or the plasma source configuration such as Ref. 17.

The merits of usage of this high power inverter unit are that due to the skin depth effect[16], it can be expected that high density ($10^{18} \sim 10^{19}$ m^{-3}) of plasma is produced, and that more RF power will be absorbed to the excited plasma than that to RF plasmas ignited by conventional RF supplies. In this work, the 9-turn loop antenna, which excites the azimuthally symmetric RF electromagnetic field (m = 0 helicon mode), is chosen because of its simplicity. So far, many antennas such as helical antenna and Boswell antenna have been proposed and employed[17]. Since those antennas generate different helicon modes from the loop antenna, for example, m = 1 by the right helical antenna, m = -1 by the left helical antenna, and both m = 1 and -1 by the Boswell antenna, selecting the optimized RF antenna may be able to ameliorate the production efficiency and/or power coupling.

The efficient usage of the magnetic nozzle is also necessary. As shown in Fig. 1, the magnetic coil is located just over the RF antenna. Hence, the field works only a diverging nozzle. In general, it is difficult to make a supersonic flow, and a diffuser (diverging nozzle) works as a decelerating nozzle for a subsonic flow while a converging nozzle works as an accelerating nozzle. For that, to make a subsonic flow a supersonic flow, a diverging nozzle is often used in combination with a converging nozzle, which is called Laval nozzle. The same physics as the solid nozzle, the isentropic theory, should be held on the magnetic nozzle as well. And yet, it is possible that the assumption of the mass conservation will be failed because of the cross-field diffusion. Thus, positions of the RF antenna and of the solenoid coil need to be reconsidered to duplicate the configuration of the Laval nozzle using the magnetic field. Adjustment of those positions can address not only the issue of the thrust enhancement, but also that of effective plasma transportation downstream.

IV. Conclusion

A new type of thruster using a high power FET-based inverter power supply with 90% of the DC to RF conversion efficiency is constructed. The system is driven around 300 kHz, which is much lower than that used in other RF plasma thrusters. To evaluate the performance of this new thruster, thrust forces are mainly and directly measured using the plate type thrust target. The maximum value of 19.7 mN is obtained when the input RF power is 16.4 kW and 27.4 mT of the magnetic field is applied. Then, acquired plasma densities are 7×10^{18} m^{-3} in the source tube and 4×10^{17} m^{-3} at the target position, respectively. On the other hand, the obtained thrust power ratio is only 1.2 mN/kW, and much plasma loss is observed. Therefore, to enhance the performance, it is necessary to design the plasma source configuration, the position of an RF antenna, and the magnetic field configuration for the plasma acceleration in a magnetic nozzle and more effective transportation of plasma downstream.

Acknowledgments

This work was supported in part by a Grant-in-Aid for Scientific Research from the Japan Society for the Promotion of Science.

References

[1]Inutake, M., Ando, A., Hattori, K., Tobari, H., Makita, T., Shibata, M., Kasashima, Y., and Komagome, T., "Generation of Supersonic Plasma Flows Using an Applied-Field MPD Arcjet and ICRF heating," *Plasma Physics and Controlled Fusion*, Vol. 49, pp. A121 - A134, 2007.

[2]Mazouffre, S., Tsikata, S., and Vaudolon, J., "Development and Experimental Characterization of a Wall-less Hall Thruster," *Journal of Applied Physics*, Vol. 116, paper 243302, 2014.

[3]Toki, K., Kuninaka, H., Nishiyama, K., Shimizu, Y., and Funai, I., "Technological Readiness of Microwave Ion Engine System for MUSES-C Mission,"*Proceedings of the 27th International Electric Propulsion Conference*, IEPC-01-174, 2001.

[4]Andres, M., C., P., and Nikolai, T., "The VASIMR Engine: Benefits, Drawbacks, and Technological Challenges," *Proceedings of the 32nd International Electric Propulsion Conference*, IEPC-2011-251, 2001.

[5]Charles, C., "A Riview of Recent Laboratory Double Layer Experiments," *Plasma Sources Science and Technologies*, Vol. 16, No. 4, R1, 2007.

[6]Takahashi, K., Charles, C., Boswell, R. W., and Fujiwara, T., "Electron Energy Distribution of a Current-Free Double Layer: Druyvesteyn Theory and Experiments," *Physical Review Letters*, Vol. 107, No. 3, paper 035002, 2011

[7]Takahashi, K., Lafleur, T., Charles, C., Alexander, P., and Boswell, R. W., "Electron Diamagnetic Effect on Axial Force in an Expanding Plasma: Experiments and Theory," *Physical Review Letters*, Vol. 107, No. 23, paper 235001, 2011

[8]Takahashi, K., Lafleur, T., Charles, C., Alexander, P., and Boswell, R. W., "Approaching the Theoretical Limit of Diamagnetic-Induced Momentum in a Rapidly Diverging Magnetic Nozzle," *Physical Review Letters*, Vol. 110, No. 19, paper 195003, 2011

[9]Takahashi, K., Chiba, A., Komuro, A., and Ando, A., "Axial Momentum Lost to a Lateral Wall of a Helicon Plasma Source," *Physical Review Letters*, Vol. 114, No.19, paper 195001, 2015

[10]Ando, A., Komuro, A., Matsuno, T., Tsumori, K., and Tekeiri, Y., "Radio Frequency Ion Source Operated with Field Effect Transistor Based Radio Frequency System," Review of Scientific Instruments, Vol. 81, pp. 02B107-1 – 02B107-3, 2010.

[11]Ando, A., Matsuno, T., Funaoi, T., Tanaka, N., Tsumori, K., and Takeiri, Y., "Characteristics of Hydrogen Negative Ion Source with FET based RF System," *American Institute of Physics Conference Proceedings*, Vol. 1390, No. 1, pp. 322-329, Sept., 2011

[12]Chiba, A., Takahashi, K., Komuro, A., and Ando, A., "Characterization of Helicon Plasma Thruster Performance Operated for Various Rare Gas Propellants," *Journal of Propulsion and Power*, Vol. 31, No. 3, pp. 962-965, 2015

[13]Charles, C., Boswell, R., and Takahashi, K., "Boltzmann expansion in a radiofrequency conical helicon thruster operating in xenon and argon," *Applied Physics Letters*, Vol. 102, No. 22, paper 223510, 2013

[14]Georg, H., F., Keller, A., Braxmaier, C., and Tajmar, M., "Development of a Highly Precise Micronewton Thrust Balance," *IEEE Transactions on Plasma Science*, Vol. 43, No. 1, pp. 234 – 239, 2015

[15]Takahashi, K., Komuro, A., and Ando, A., "Measurement of Plasma Momentum Exerted on Target by a Small Helicon Plasma Thruster and Comparison with Direct Thrust Measurement," *Review of Scientific Instruments*, Vol. 86, No. 2, pp. 322-329, Feb., 2015

[16]Takahashi, K., Charles, C., Boswell, R., and Ando, A., "Effect of Magnetic and Physical Nozzle on Plasma Thruster Performance," *Plasma Source Science and Technology*., Vol. 23, paper 044004, 2014

[17]Charles, C., Takahashi, K., and Boswell, R., W., "Axial Force Imparted by a Conical Radiofrequency Magneto-Plasma Thruster," *Applied Physics Letters*, Vol. 100, No. 11 pp. 113504-1 – 113504-3, 2012

[18]Hoshino, Y., Ishiyama, T., Komuro, A., Takahashi, K., and Ando, A., "Development of 15 kW Class RF Plasma Source for VASIMR Type Space Propulsion with Magnetic Nozzle," *Plasma Fusion and Research, in press*.

[19]Chen, F., F., "Helicon Discharges and Sources: A Review," *Plasma Sources Science and Technology*, Vol. 24, No. 1, paper 014001, 2015